Heliyon 10 (2024) e30943

Contents lists available at ScienceDirect

Heliyon

journal homepage: www.cell.com/heliyon

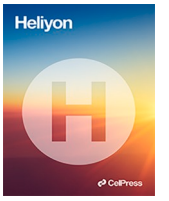

Research article

Tantalum-doped tin oxide thin films using hollow cathode gas flow sputtering technology

Fangfang Huo [a,*], Ruslan Muydinov [a], Bertwin Bilgrim Otto Seibertz [a], Can Wang [b,c,d], Manuel Hartig [a,e], Nivin Alktash [a], Peng Gao [b,c,d], Bernd Szyszka [a,**]

[a] Institute für High-Frequency and Semiconductor-System Technologies, Technische Universität Berlin, Einsteinufer 25, 10587, Berlin, Germany
[b] CAS Key Laboratory of Design and Assembly of Functional Nanostructures, and Fujian Provincial Key Laboratory of Nanomaterials Fujian Institute of Research on the Structure of Matter, Chinese Academy of Sciences, 350002, Fuzhou, Fujian, China
[c] Laboratory for Advanced Functional Materials, Xiamen Institute of Rare Earth Materials, Haixi Institute, Chinese Academy of Sciences, 361021, Xiamen, China
[d] University of Chinese Academy of Sciences, 100049, Beijing, China
[e] PvcomB, Helmholtz-Zentrum Berlin für Materialien und Energie GmbH, Schwarzschildstraße 3, 12489, Berlin, Germany

ARTICLE INFO

Keywords:
SnO_2
Gas flow sputtering (GFS)
Ta
O_2 flow
Transparent conductivity

ABSTRACT

SnO_2 and tantalum doped SnO_2 (TTO) thin films were prepared using reactive hollow cathode gas flow sputtering (GFS) on glass substrates. An in-situ heating process under vacuum preceded the sputtering. The resistivity of the tin oxide films was reduced to a remarkable low of 2.02×10^{-3} Ω cm, with a carrier concentration of 2.55×10^{20} cm^{-3} and a mobility of 12.11 $cm^2V^{-1}s^{-1}$. As the substrate temperature increased, the film resistivity decreased. Notably, at a substrate temperature of 270 °C, the effect of Ta doping on the film resistivity and carrier concentration was significantly stronger compared to higher temperatures. Elevating the substrate temperature and Ta doping resulted in a lower refractive index (n). This effect was consistently strong at higher temperatures, attributed to the higher film-free carrier concentration (4.54×10^{20} cm^{-3}) compared to lower temperatures (2.35×10^{20} cm^{-3}). The film's structure was characterized by scanning electron microscopy (SEM), X-ray diffraction (XRD) and atomic force microscope (AFM). The preferred direction of film growth was discussed. The successful and reproducible fabrication of tin oxide films underscores the advantages of gas flow sputtering (GFS) technology. GFS offers stable operating conditions across various oxygen flow levels without requiring target oxidization control, as is required in magnetron sputtering when managing gas status and film quality.

1. Introduction

Transparent conducting oxides (TCOs) have been widely used in many areas, especially photo electronic semiconductor devices [1,2]. Starting with the early work in 1983 [3], SnO_2 has shown to be an excellent semiconductor for such applications due to its band gap of 3.62 eV at 298 K with high transparency in the UV–Visible region and its low electrical resistance. Thus, SnO_2 has been proposed as a potential candidate for photo-electrodes [4,5], flexible transparent heater [6], gas sensing devices [7,8], solar cells [9–11], which has a

* Corresponding author.
** Corresponding author.
E-mail addresses: fangfang.huo@tu-berlin.de (F. Huo), bernd.szyszka@tu-berlin.de (B. Szyszka).

https://doi.org/10.1016/j.heliyon.2024.e30943
Received 19 January 2024; Received in revised form 5 May 2024; Accepted 8 May 2024
Available online 10 May 2024

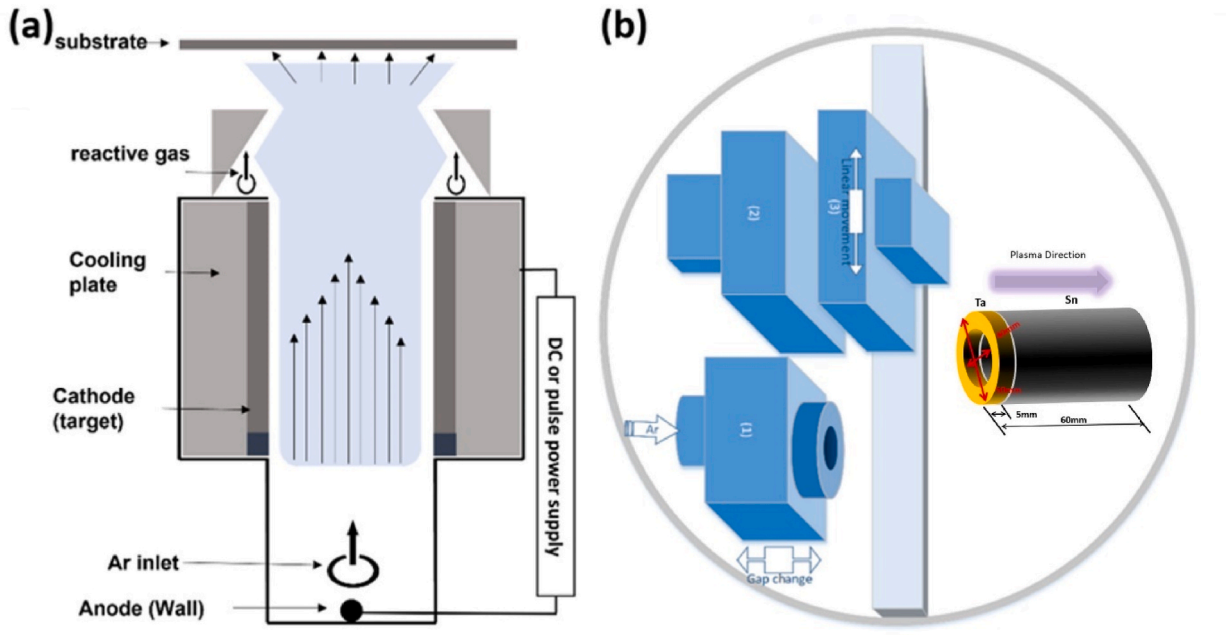

Fig. 1. (a) Schematic of hollow cathode gas flow sputtering (GFS) technology, (b) Structure of vacuum sputtering chamber: source (1), pre-heating (2), and substrate holder (3). Insert is a 3D target used in the GFS system.

high transmittance, low resistivity, and stable performance.

The most important advantage is that the raw materials are naturally abundant and environmentally friendly. All these additional desirable properties make SnO_2 applicable to a broader range of applications than traditional TCOs, like indium tin oxide (ITO) due to a shortage of indium [12], and fluorine-doped tin oxide (FTO) with high surface roughness due to fabrication process [13]. Until now, various techniques to prepare TTO thin films have been reported. For example, tin oxide thin films have been prepared by chemical solution process [14], electron beam evaporation [15], magnetron sputtering [16], sol-gel method [17], chemical vapor deposition [18] and atomic layer deposition [19] and so on. Reactive sputtering deposition offers more freedom to adjust stoichiometry, microstructure, and properties by controlling the composition of the target, reactive gas, and deposition conditions [20].

Like other n-type semiconductor materials, the electrical property of SnO_2 can also be optimized by extrinsic dopants [1]. Fluorine (F), Antimony (Sb) [21], niobium (Nb), and tantalum (Ta) are mostly used as doping agents (donor materials) to achieve high n-type conductivity while maintaining high optical transparency. Theoretically, the ideal donor dopant for SnO_2 should therefore be of a similar ionic radius to Sn, sits in a state with a high conduction band, but not hybridize with the host Sn 5s states while being in the correct oxidation state. The close ionic radii could avoid structural defects caused by replacing Sn^{4+} with donor ions. A correct or suitable oxidation state will give extra free electrons to the SnO_2 lattice through interstitial or substitutional doping to increase the electrical conductivity, optical transmittance, and IR reflectivity [22]. A higher conduction band means a small energy difference exists between the donor energy level and the conduction band of SnO_2. Then less energy is required by the electrons to reach the conduction band. Nb doping of SnO2 has demonstrated moderate results experimentally, with high mobilities for SnO_2 but suffering from low carrier concentrations, in most cases failing to reach 1×10^{20} cm^{-3} [23]. Furthermore, the carrier mobility in sputtered Sb doped SnO_2 (ATO) is limited by ingrain and grain boundary scattering during DC magnetron sputtering process, which suffers from the high energy ion bombardment and yields polycrystalline films with small grain size [24]. It is also found that both Sb and F hybridize with the conduction band minimum (CBM), thus providing a detrimental effect to the band curvature with increased doping concentrations, and that Ta does not undergo this same effect, with that Ta could increase the film mobility [23].

Besides via doping to optimize the tin oxide film electrical property, it could also be possible to fabricate bi-layer or multilayer structure to improve film property. Compared with the property of single tin oxide films, the multi-structure transparent conductive films (TCFs) based on tin oxides could achieve higher conductivity [25,26]. It is also a good direction to develop SnO_2 films in this work with nanowires in the future. Shihui Yu group found that flexible transparent conductive film Ag@SnO_2 core-shell nanowire (Ag NW@SnO_2) shows low sheet resistance of 9.3 Ω/sq with ~85.3 % of optical transmittance [27], and an ultrathin, hybrid NMs consisting of a silver nanowire network with tin oxide shell with low sheet resistance of 9.6 Ω/sq which could be conformal attached to human skin [14]Also the application of Sb doped SnO_2 (ATO) covering layer to improve the performances of CuNWs on polyethylene terephthalate (PET) substrate was studied, a power conversion efficiency (PCE) of 6.39 % for Polymer solar cells (PSCs) was gained, which is higher than that of PSCs using ITO (5.87 %) [11]. Furthermore, a flexible tri-layers of ATO/AgNWs/ATO films show a high figure of merit value (30.06×10^{-3} Ω^{-1}) with a low sheet resistance of 7.1 Ω/sq deposited on flexible substrate [28], and other oxides related multilayer structure were also well studied [29–34]. These findings provide that Cu and Ag NWs could improve the single SnO_2 layer electrical property [35], also proves that tin oxide based TCOs have a great potential to replace commercial ITO and FTO [36].In

Table 1
Deposition parameters for tin oxide films.

Parameter		Value
Target		Sn (purity: 99.99 %), Ta (purity: 99.99 %)
Substrate		3 mm SGG PLANICLEAR glass air side
Power		250 W
Pulse mode	reverse voltage	100 V
	frequency	100 KHz
	time	2 μs
Distance		4 cm
In situ substrate temperature		RT, 50 °C, 110 °C, 270 °C, 400 °C
Ar		1000 sccm (purity: 99.999 %)
O_2		5–45 sccm (purity: 99.999 %)

this study, a novel method was used to prepare the transparent conductive tin oxide films, a Hollow Cathode Gas Flow Sputtering (GFS) technology [37], which is also successful for 'soft' growth ZnO films on sensitive substrate material [38]. Although extensive knowledge and research are available on SnO_2 and doping SnO_2 films fabrication, especially for SnO_2 fabricated by DC/RF magnetron sputtering, little is known about the plasma generating process and corresponding working gas flow rate of sputtering on growth and property of tin oxide layers by reactive hollow cathode gas flow sputtering (GFS) technique. Unlike magnetron sputtering, magnet part is not necessary in hollow cathode gas flow sputtering technology to confine the particles near the surface of the target, plasma could be generated inside the target and goes through directly to the surface of the substrate. A schematic of the hollow cathode gas flow sputter process is shown in Fig. 1. In addition to high film quality and good reproducibility, its advantages with respect to magnetron sputtering also include high deposition rate due to the high sputter yield of metallic the target, lower request of vacuum background pressure, and low deposition temperature, which will offer an essential technical basis in defects controlling in a wide range and properties optimization. Where due to the high plasma density at the substrate in reactive GFS (plasma density at the substrate in the order of $n_i = 10^{12}$ cm^{-3} for reactive GFS [39] compared to $n_i \leq 10^9$ cm^{-3} for reactive magnetron sputtering [40]), a substantial improvement of surface diffusion and thus improved access to polycrystalline and even epitaxial film growth can be expected. It would be highly desirable that such a low-cost coating route could be applied to fabricate high-quality TTO with improved transparent conductivity, thus helping to offer a new window with potential low-cost alternative transparent electronic material for large area photonic applications.

2. Experimental details

2.1. Deposition process

Tin oxide films were deposited on Saint Gobain PLANICLEAR glass by hollow cathode gas flow sputtering using pure tin (Sn) metal ring and tantalum metal (Ta) ring, purity of 99.999 %. Before deposition, glasses were ultrasonically cleaned in deionized water, ethanol, and isopropanol for 15 min, respectively, at room temperature. The distance between the target and substrate was 4 cm. The background pressure in the deposition chamber before sputtering was held around 2×10^{-2} mbar; during sputtering was held at 3.2×10^{-1} mbar, which is easier to reach compared with magnetron sputtering. To use the reactive GFS for its extraordinary process stability compared to reactive magnetron sputtering, where process conditions can be tailored and stabilized without hysteresis and the need for transition mode process control.

Fig. 1 shows the schematic of the hollow cathode gas flow sputtering (GFS) system used in this work and the principle of gas flow sputtering technology [41]. By voltage application, a glow discharge with a high plasma density occurs inside the hollow cathode. The sputtered material is effectively transported by argon gas flow to the outlet of the hollow cathode towards the surface of the substrate, where O_2 is realized (no target poisoning), and the sputtered atoms can react with some of the offered O_2 and build the film at the substrate surface. Additional magnetic fields, as in magnetron configurations, are not necessary. Pure 5 N argon was used as sputter gas to generate plasma and through hollow cathode (targets), transport the sputtered material towards the substrate. 5 N Oxygen was used as a reactive gas to react with atoms from the target surface to produce different compositions and preferred structured films. A comparably high process pressure and, therefore, the high charge carrier concentration led to a power density, enabling a high plasma density and an intense sputter erosion of the target. Fig. 1b shows the structure of the vacuum sputtering chamber. During the deposition process, the sample is fixed on the substrate holder (SH) (3) and can be heated from the substrate holder and the pre-treatment station (2). Then the substrate holder moves in front of the sputter source (1) to start the deposition. Insert Fig. 1b shows the 3D target used in this work, named hollow cathode in the GFS system. The shape of the target matches the size of the opening in the actively cooled cathode of the sputter source, so the argon flux and generated plasma are passing throughthe hollow target and deposit a film on the substrate.

Table 1 shows the detailed deposition parameters during sputtering. Two major variations are in situ substrate temperature and oxygen flow rate. The tin and air sides of the SGG PLANICLEAR glass substrate were checked before deposition, and films are always deposited on the air side.

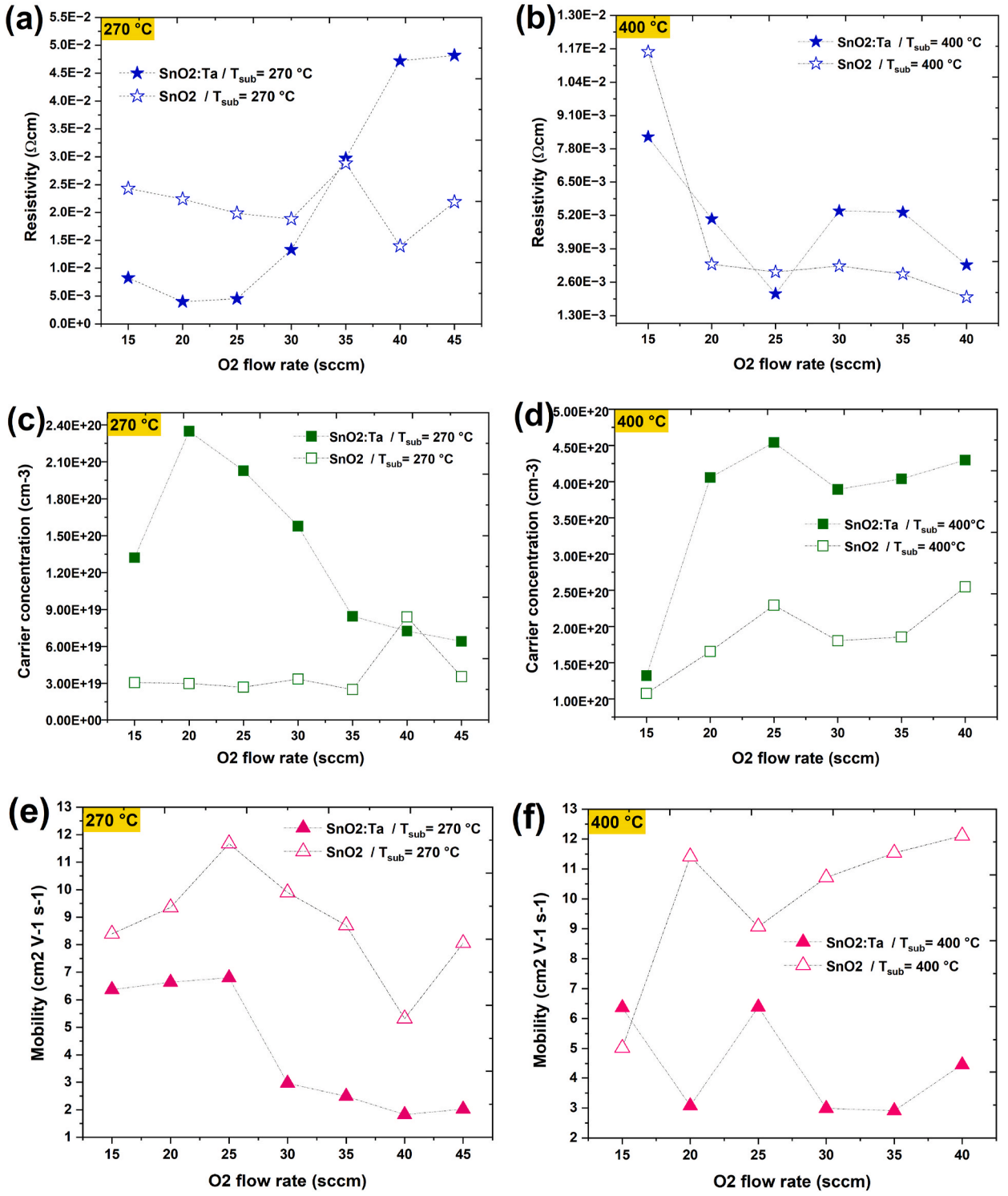

Fig. 2. Comparison of hall measurement results: resistivity (ρ), carrier concentration (ne) and mobility (μ) of SnO_2 and SnO_2: Ta films deposited at different O_2 flow rates and different substrate temperature.

2.2. Materials characterization and measurement methods

X-ray diffraction (XRD) was conducted at Bragg-Brentano setup θ-2θ scan in the air using a Bruker D8 Discover diffractometer in the range 20–70° with monochromatic Cu Ka1 and Ka2 radiation (1.54056 and 1.54439 Å respectively) under voltage 40 kV and current 40 mA. The composition of Ta-doped SnO_2 film characterization was detected by wavelength dispersive x-ray (WDX) spectroscopy technique. The surface morphology of the films was analyzed using a LEO GEMINI 1530 field emission scanning electron microscope (FESEM). The topology was investigated by an atomic force microscope (AFM) using a NT-MDT Ntegra II with μMash NSC15 tips (radius 8 nm or smaller) in tapping mode. Electrical characterization of sheet resistance (Rsh) and detailed hall info, including resistivity ρ, hall mobility μ, and free carrier density ne, were performed by a four-point probe and hall measurement. Optical transmittance and reflectance were carried out in the 250–2450 nm wavelength range using a PerkinElmer Lambda UV/VIS/NIR spectrometer. Film thickness was evaluated by ellipsometry. All the measurements were performed at room temperature.

3. Result and discussion

3.1. Electrical and optical properties

Electrical properties of tin oxide films were measured under room temperature with the hall device. Resistivity (ρ), carrier concentration (n_e), and mobility (μ) of SnO_2 and SnO_2: Ta films deposited with different substrate temperature are shown in Fig. 2, and it was observed that films deposited with a lower substrate temperature than 270 °C are not conductive. As is shown in Fig. 2a, for SnO2 films deposited on 270 °C heated substrate, film's resistivity (ρ) stays around 2×10^{-2} Ω cm with the increasing of O_2 flow rate. After doped with Ta, films resistivity (ρ) decreased at first when O_2 flow rate increased, at 20 sccm O_2 flow rate reached the lowest value 4.01×10^{-3} Ω cm, and then keep a low value 4.53×10^{-3} Ω cm at 25 sccm O_2 flow rate. Ta doping decreased film resistivity is related to the donor Ta which could provide one more extra electron (e^-) in Sn–Ta–O system, since tetravalent Sn was replaced by pentavalent element Ta and during the covalent bond forming process with oxygen, one of the five outer electrons from Ta will lose to be a free electron (e^-) to conduction band. However, as oxygen flow continues to increase, the number of oxygen vacancy became excessively large, which weakened Ta donor effect, film resistivity increased, film conductivity became worse, and it was also observed that film structure degraded at higher O_2 flow rate, which is shown the XRD pattern of films in Fig. 7a. That also explains why the carrier concentration (n_e) of SnO_2: Ta film is higher than SnO_2 film, and with the increasing with O_2 flow rate over than 20 sccm, SnO_2: Ta film's carrier concentration (n_e) decreased. As is shown in Fig. 2c, carrier concentration (n_e) of SnO_2 film stays around 3×10^{19} cm^{-3} with different O_2 flow rates. For SnO_2: Ta film, carrier concentration increased with the increasing O_2 flow rate, at 20 sccm O_2 flow rate reached the highest value 2.35×10^{20} cm^{-3}. Regarding film mobility (μ), which is shown in Fig. 2e, there is an inverse tendency with Ta doping and changing of O_2 flow rate compared with resistivity (ρ). For SnO_2 and SnO_2: Ta films, the inflexion points both come at 25 sccm O_2 flow rate, film mobility (μ) is 11.7 $cm^2 V^{-1} s^{-1}$ and 6.8 $cm^2 V^{-1} s^{-1}$. The inverse tendency of mobility (μ) with changing of O_2 flow rate could explain by the relationship of (ρ), carrier concentration (n_e), and mobility (μ):

$$\rho = \frac{1}{q n_e \mu} \tag{1}$$

As is known, charge carrier mobility (μ) in transparent conductive oxide (TCO) is described by the scattering mechanisms in Matthiessen's rule:

$$\frac{1}{\mu} = \sum_i \frac{1}{\mu_i} = \frac{1}{\mu_{impurity}} + \frac{1}{\mu_{gb}} + \frac{1}{\mu_{hopping}} + \frac{1}{\mu_{phonon}} + \ldots \tag{2}$$

where $\mu_{impurity}$, μ_{gb}, $\mu_{hopping}$, and μ_{phonon} are factors that influence mobility from impurity scattering, grain boundary scattering, retardation by hopping transport, and phonon scattering, respectively. In our case, Ta doping decreased film mobility (μ) results from the impurity and grain boundary scattering since the changing of SnO_2 lattice structure by Ta element intergration, and with the increasing of O_2 flow rate, oxygen vacancy becomes excessively large, which interferes with scattering of electrons and disturbs electron mobility.

For films deposited with a higher substrate temperature at 400 °C, resistivity (ρ), carrier concentration (n_e), and mobility (μ) of SnO_2 and SnO_2: Ta films are shown in Fig. 2b–d and f respectively. With a higher substrate temperature, SnO_2 film resistivity (ρ) decreased from 1.2×10^{-2} Ωcm to 3.3×10^{-3} Ωcm when O_2 flow rate increased from 15 sccm to 20 sccm, and with the increasing of O_2 flow rate, film resistivity (ρ) keeps at the same order 10^{-3} Ωcm, which is lower than SnO_2 film with a 270 °C substrate temperature. That results from a higher substrate temperature could get a larger grain size, and increasing the grain size could reduce resistivity (ρ) in SnO_2 films, which is also confirmed that grain boundaries (GBs) play an important role in modulating the ρ value in polycrystalline films [42,43] Film grain size was analyzed with XRD pattern in Fig. 2. After doping with Ta, film resistivity (ρ) was not reduced obviously and like what it is observed with a 270 °C substrate temperature. At only 25 sccm O_2 flow rate, SnO_2: Ta film resistivity is lower than SnO_2 film, which is 2.1×10^{-3} Ωcm of SnO_2: Ta film and 3×10^{-3} Ωcm of SnO_2 film. For carrier concentration (n_e), SnO_2 and SnO_2: Ta films both get a higher carrier concentration at 10^{20} cm^{-3} order when deposited with a higher substrate temperature, and the highest value was both reached at 25 sccm O_2 flow rate, which is 4.54×10^{20} cm^{-3} of SnO_2: Ta film and 2.29×10^{20} cm^{-3} of SnO_2 film respectively. For mobility (μ), the tendency is same as what is observed in film deposited with a lower substrate temperature, Ta doping could decrease film mobility since scattering mechanism what was discussed before, and the highest mobility value of SnO_2

Table 2
Comparison of the electrical property of SnO_2: Ta films produced in this work and literature.

Films	Target	Substrate	Deposition technique	T (°C)	ρ (Ωcm)	μ ($cm^2 V^{-1}s^{-1}$)	n_e (10^{20} cm^{-3})	Reference
TTO	ceramic	amorphous fused silica	RF-MS	600	5.4×10^{-4}	25.7	4.5×10^{20}	[44] (2016)
TTO	ceramic	Si wafer/quartz	DC-MS	400	2.0×10^{-3}	24.5	1.28×10^{20}	[45] (2021)
TTO	ceramic	amorphous fused silica	RF-MS	700	1.7×10^{-3}	12	3.3×10^{20}	[46] (2014)
TTO	SnO_2, Ta_2O_5	soda-lime glass	RF co-sputtering	400	8.5×10^{-3}	16.6	4.4×10^{19}	[47] (2018)
TTO	SnO_2, Ta	Corning glass	MS co-sputtering	270	2.1×10^{-3}	14.4	2.1×10^{20}	[48] (2017)
TTO	SnO_2, Ta	fused silica/silicon	MS co-sputtering	400	$2.44 \times 10\text{-}^{3}$	8.62	2.97×10^{20}	[49] (2021)
SnO2	Sn	Glass	MS	25	conductivity (σ) 4 S/m	–	–	[50] (2023)
SnO2	SnO	FTO	RF-MS	200[a]	1.34×10^{-1}	11.29	–	[51] (2023)
SnO2	Sn	SGG PLANICLEAR glass	Gas Flow Sputtering (GFS)	400	2.02×10^{-3}	12.11	2.55×10^{20}	This work
TTO	Sn, Ta	SGG PLANICLEAR glass	Gas Flow Sputtering (GFS)	400	2.15×10^{-3}	6.39	4.54×10^{20}	This work
TTO	Sn, Ta	SGG PLANICLEAR glass	Gas Flow Sputtering (GFS)	270	4.01×10^{-3}	6.63	2.35×10^{20}	This work

[a] Substrate temperature is 200 °C, then sample annealed at 250 °C in air for 30 min.

film which was observed at 40 sccm O_2 flow rate is 12.1 $cm^2V^{-1}s^{-1}$. For SnO_2: Ta film, the highest mobility value was observed at 25 sccm O_2 flow rate, which is 6.4 $cm^2V^{-1}s^{-1}$. So it could be inferred that Ta doping effect in SnO_2 films is largely influenced by substrate temperature and O_2 flow rate, when substrate temperature is high, grain size of host material becomes large, Ta doping effect is weakened, however, Ta could still provide free electron (e^-) to Sn–Ta–O system, so the resistivity of SnO_2: Ta film at 25 sccm O_2 flow rate is lower than that of SnO_2 film results from a proper fit with oxygen vacancy, and this could also explain why the carrier concentration (n_e) of SnO_2: Ta film is higher than that of SnO_2 film. This is also confirmed that grain boundary and oxygen vacancy are two key factors in modulating electrical properties in tin oxide films.

Table 2 summarizes the electrical property of TTO films prepared by magnetron sputtering technology and this work, the lowest resistivity was achieved at 5.4×10^{-4} Ω cm by Mirko Weidner in 2016, using a ceramic target with a substrate temperature at 600 °C [44]. Compared with magnetron sputtering, SnO_2 film with a resistivity of 2.02×10^{-3} Ω cm without doping in this work can be achieved at a lower substrate temperature of 400 °C, which is higher than that of Ta doped SnO_2 film, 2.15×10^{-3} Ω cm. The reason could be related to the crystal structure changing with higher temperature in case GFS technology has higher plasma density than magnetron sputtering. Furthermore, with a lower substrate temperature of 270 °C, a low resistivity of 4.01×10^{-3} Ω cm can also be gained in Ta doped SnO_2 film. With GFS technology, Ta doping could get a similar effect as high temperature during SnO_2 films deposition. In the future, another Ta doping concentration under different temperatures will be further researched.

As is shown in Fig. 3a–b, in visible range, transmittance of SnO_2 and Ta doped SnO_2 films with substrate temperature of 270 °C are both > 80 %. With increasing of the substrate temperature to 400 °C, film transmittance decreased slightly, and transmittance of Ta doping SnO_2 films is lower than that of SnO_2 films. In infrared range, Ta doping could strongly decrease the transmittance due to the transferring of photon energy to electron in conduction band, which also results in the carrier concentration of SnO_2: Ta films ($\sim 10^{20}$ cm^{-3}) is higher than that of SnO_2 films ($\sim 10^{19}$ cm^{-3}). Optical bandgap of tin oxide films are determined from Tauc plot method, which is shown in Fig. 3c and d. A higher substrate temperature could enlarge the film bandgap. The largest bandgap of SnO_2 film with 400 °C substrate temperature is 3.78 eV. However, compared with substrate temperature of 400 °C, Ta doping could enlarge the bandgap of tin oxide films at 270 °C, for example, at O_2 flow rate 20 sccm, SnO_2: Ta film get a same bandgap as SnO_2 film at 30 sccm. Considering the film resistivity, SnO_2: Ta film (4.01×10^{-3} Ω cm) is lower than that of SnO_2 film (1.88×10^{-2} Ω cm), so it could be concluded that though higher temperature substrate could get a lower resistivity tin oxide film, film transmittance decreased, and higher temperature deposition needs more heating time and energy cost. With 270 °C substrate temperature at 20 sccm O_2 flow rate, using Ta doped SnO_2 film is a good way to produce high property tin oxide films.

To better understand the relationship between film optical property and free carrier, also the relationship with film conductivity, optical constants refractive index (n) and extinction coefficient (k) of tin oxide films with low resistivity (10^{-3} Ω cm) are shown in Fig. 4 a and b, which are both measured by ellipsometry at 550 nm wavelength. With higher substrate temperature, a lower refractive index (n) can be gained. And this phenomenon matched with hall measurement free carrier concentration result, that tin oxide film with 400 °C substrate is higher than that of 270 °C. As it is known, refractive index (n) and extinction coefficient (k) are associated with film reflection and absorption. Basically, a lower refractive index and extinction coefficient improve light management and minimize the light loss induced at the interface. For instance, Eun Joo Yeom et al. found that transparent Sn-based film used as ETL in perovskite solar cells could increase the absorption of perovskite film, and optimize cell property, due to more efficiently using incident light than TiO_2 film, which has a higher refractive index than SnO_2.

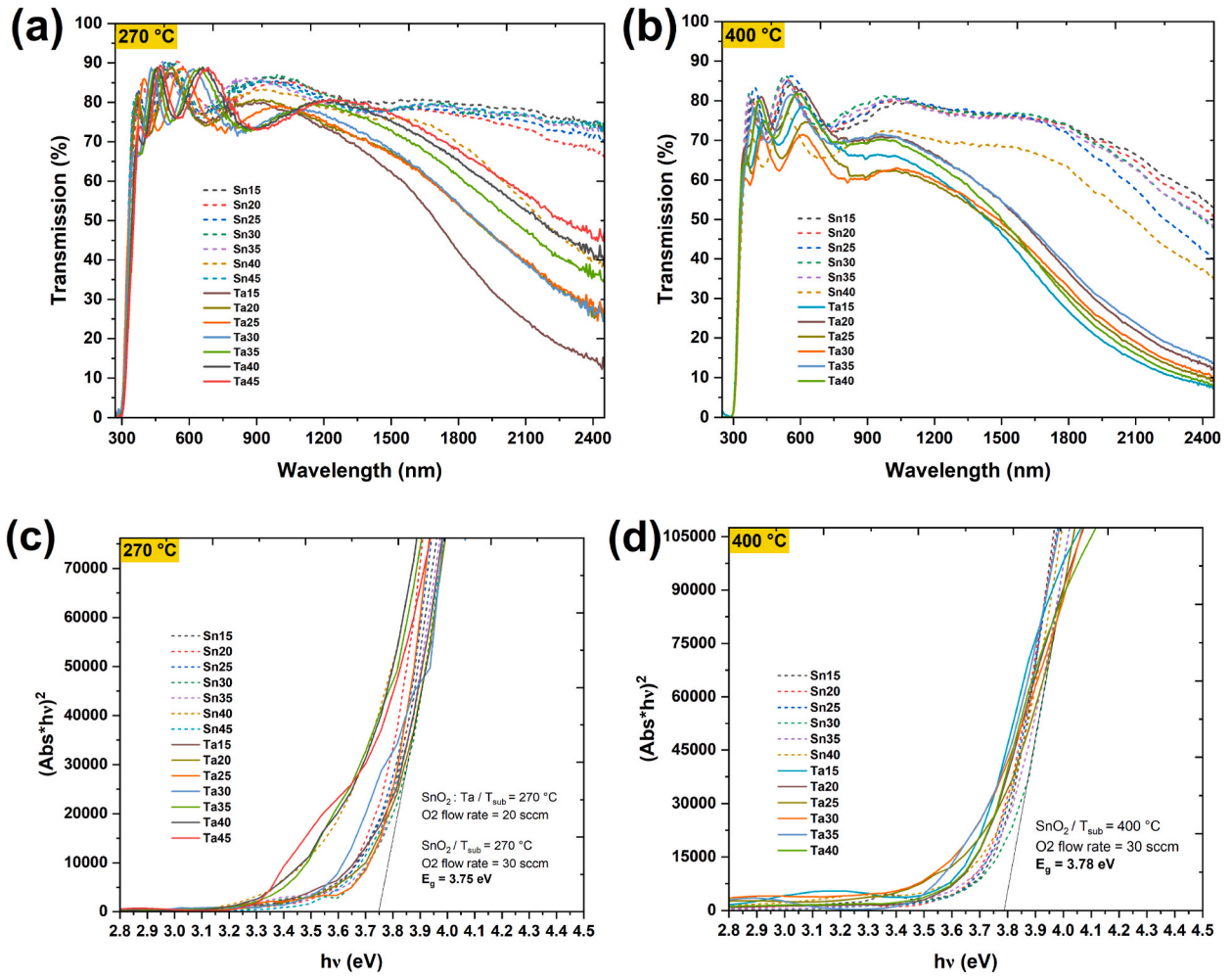

Fig. 3. Transmittance spectra of tin oxide films deposited at different O_2 flow rate with substrate temperature of (a) 270 °C and (b) 400 °C. Optical bandgap of tin oxide films calculated by Tauc plot with different substrate temperature (c) 270 °C and (d) 400 °C corresponding to the films in (a) and (b).

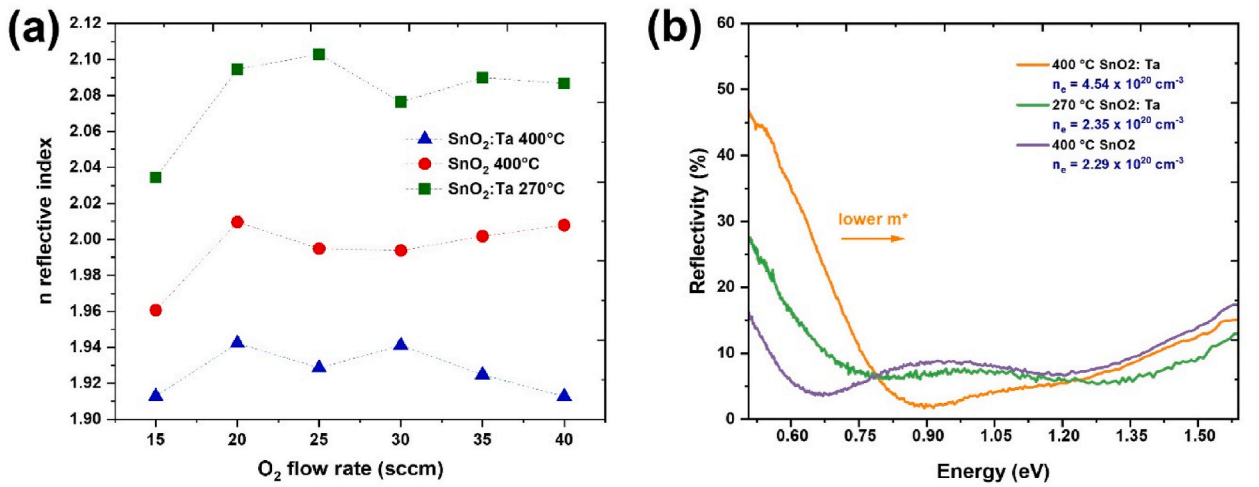

Fig. 4. Optical constants refractive index n value (a) of tin oxide films measured by ellipsometry at 550 nm wavelength and (b) the IR reflectivity spectra of tin oxide samples.

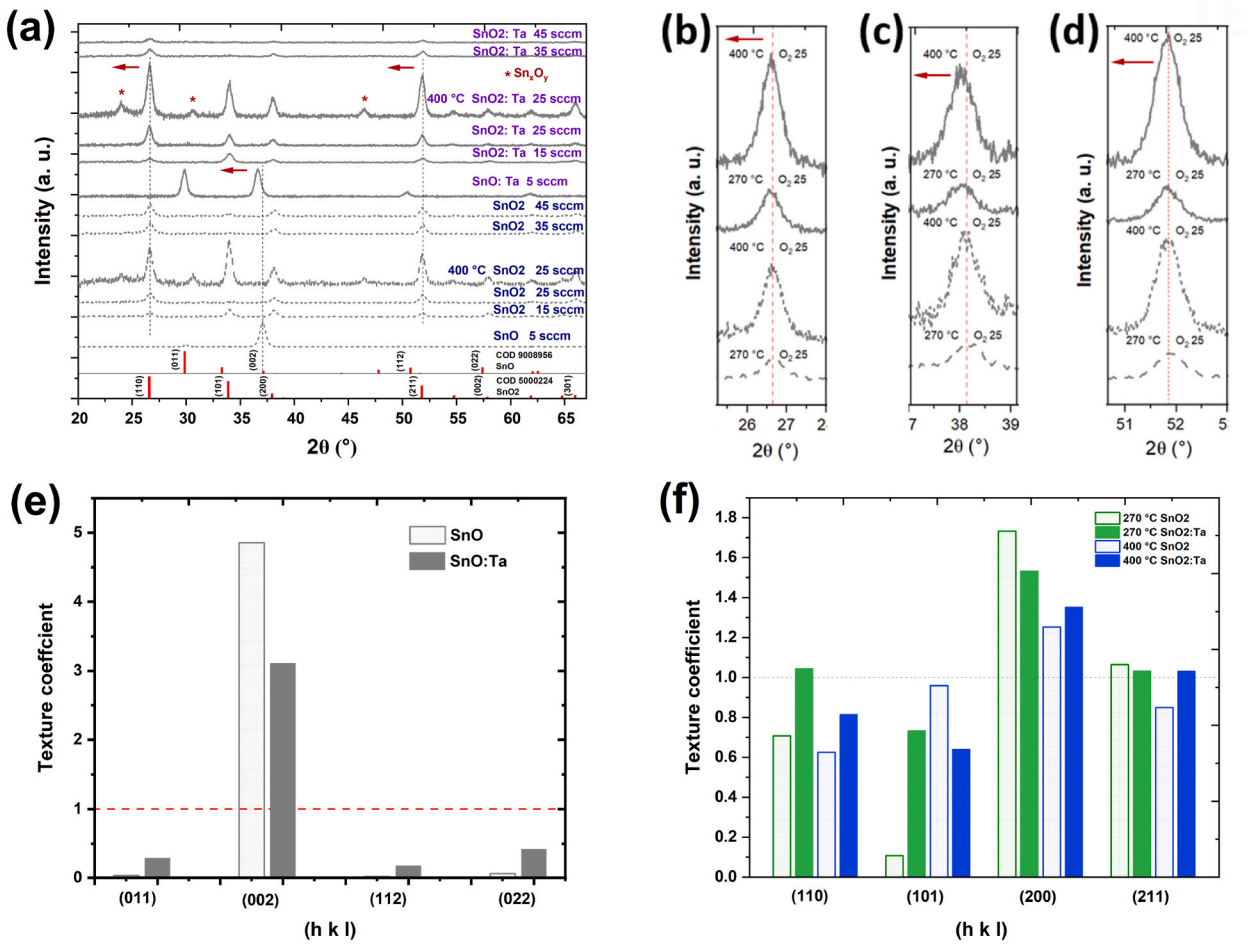

Fig. 5. (a) XRD pattern of tin oxide films deposited at different O_2 flow rates on substrate temperature of 270 °C, and films deposited at 25 sccm O_2 flow rate on substrate temperature of 400 °C, the dotted line is the undoped film, the solid line is Ta doped film, the below is reference COD 9008956, SnO romarchite structure and reference COD 5000224 SnO_2 cassiterite structure respectively. The effect of Ta doping on (110) (b), (200) (c) and (211) (d) orientations respectively. Texture coefficient of SnO (e) deposited at 5 sccm O_2 flow rate on substrate temperature of 270 °C and SnO_2 (f) films deposited at 25 sccm O_2 flow rate on different substrate temperature.

Infrared reflectivity is related to the scattering of light by free carriers in the near IR range, which also corresponds to free carrier absorption, which is affected by static imperfections (impurity, interface) and dynamic disturbances (phonon, plasma, etc.). This could also be discussed by the free carrier scattering mechanism in the conductivity phenomenon. The reflectivity spectra in the near IR range for SnO_2 and SnO_2: Ta films are shown in Fig. 4 b, which shows different onsets for plasma edge, which is determined by the plasma frequency ω_p,

$$\omega_p = \sqrt{\frac{{n_e}^2}{m^* \epsilon_\infty \epsilon_0}} \tag{3}$$

where n_e is free carrier concentration, m^* is effective mass, ϵ_∞ is the high-frequency dielectric constant, ϵ_0 is vacuum permittivity, showing that at constant carrier concentrations, the plasma frequency will depend on the inverse of the carrier effective mass [23]. Therefore, a higher plasma frequency is expected for a lower effective mass, which indicates that carriers in SnO_2 films with Ta doping and a higher substrate temperature have a higher effective mass than undoped films with a lower substrate temperature.

With the procedure doped in SnO_2 crystal structure, without forming a lot of quantity Ta_2O_5, a mix structure of Sn–Ta–O oxide and substituting Ta from Sn or Ta interstitial could create more point defect-and free electrons in the film structure. In that case, tin or oxygen vacancies are probably also formed in the structure, which lets the doping element supply more free electrons in the electrical system. In contrast, with higher temperatures, Ta and O prefer to form Ta_2O_5, therefore influencing the status of the charge carrier and decreasing the electrical conductivity of the film. This can also be related to the scattering mechanism affecting film mobility. Under higher temperatures, film mobility could be limited on grain boundary due to the lattice scattering effect.

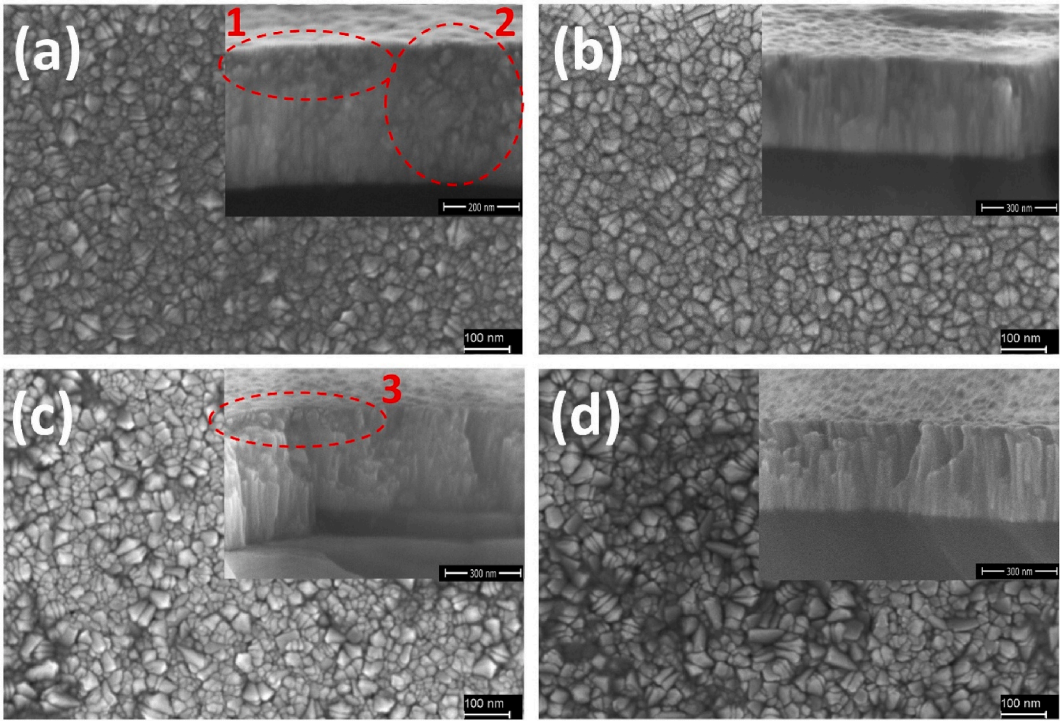

Fig. 6. Surface morphology and cross section of tin oxide films deposited with different parameters: (a) SnO_2 film with 270 °C substrate at 25 sccm O_2 flow rate; (b) Ta doped SnO_2 film with 270 °C substrate at 25 sccm O_2 flow rate; (c) SnO_2 film with 400 °C substrate at 25 sccm O_2 flow rate; (d) Ta doped SnO_2 film with 400 °C substrate at 25 sccm O_2 flow rate.

3.2. Film structure and orientation analysis

XRD patterns of sputtered tin oxide films are shown in Fig. 5a, the dotted line is undoped tin oxide film, solid line is Ta-doped tin oxide film. With increasing the substrate temperature, from room temperature to 270 °C, film structure transfers from amorphous to crystalline structure. At 5 sccm oxygen flow rate, films are confirmed with SnO romarchite structure [52]. At higher oxygen flow rate from 10 sccm to 45 sccm, films are confirmed with SnO_2 cassiterite structure [53]. Both XRD patterns of crystallized tin oxide films show that Ta doping did not change the host material structure of SnO and SnO_2. Films crystal quality increased with the O_2 flow rate increasing up to 25 sccm. However, when the O_2 flow rate is higher than 25 sccm, the crystal quality degraded due to the excessive number of oxygen vacancies. With a higher substrate temperature at 400 °C, films crystallinity increased because incoming atoms have higher diffusion lengths, and more oxygen is desorbed from the surface. Since the radius of Ta5+ is smaller than that of Sn4+, the diffractive peak of (002) moves to a smaller 2θ value in XRD pattern of SnO films. In the case of SnO_2 films, the moving of diffractive (110), (200) and (211) peaks to a smaller 2θ value could also be observed, as is shown in Fig. 2b–d. It should be noted that another phase of tin oxide was observed in XRD pattern of both tin oxide films deposited with 400 °C substrate, which were marked with three peaks by red * in Fig. 5 a, which were from intermediate oxides Sn_2O_3 (PDF 000251259)and Sn_3O_4 (PDF 000201293), that's maybe due to the sputtering process with higher substrate temperature, these two kinds of intermediate oxides were also observed in C. Guillén et al. study when sample was heated to 450 °C [54]. Considering the electrical property and Ta doping with tin oxide films with 400 °C substrate, it could be inferred that intermediate tin oxides Sn_xO_y influence the Ta doping effect with a high substrate temperature.

Texture of films were evaluated by calculating the texture coefficient ($TC_{(h_i\ k_i\ l_i)}$) using the following formula:

$$TC_{(h_i\ k_i\ l_i)} = \frac{\frac{I\ (h_i\ k_i\ l_i)}{I_0\ (h_i\ k_i\ l_i)}}{\frac{1}{n}\sum_{j=1}^{n}\frac{I\ (h_i\ k_i\ l_i)}{I_0\ (h_i\ k_i\ l_i)}} \tag{4}$$

Here, $I_{(h_i\ k_i\ l_i)}$ and $I_0\ (h_i\ k_i\ l_i)$ are the intensities of sputtered films lattice planes $(h_i\ k_i\ l_i)$ and standard references from COD 9008956, SnO romarchite structure and COD 5000224 SnO_2 cassiterite structure respectively, which are shown in Fig. 5a n denominates the total number of peaks considered for the calculation of $TC_{(h_i\ k_i\ l_i)}$. For example, n = 4 is used in SnO and SnO: Ta films due to 4 peaks are observed in XRD pattern result, which is shown in Fig. 5e, and different n were used in SnO_2 and SnO_2: Ta films because different number of peaks are observed in these XRD pattern result, and four interesting peaks [(110), (101), (200), (211)] in SnO_2 and SnO_2: Ta films are discussed in Fig. 5f. The value $TC_{(h_i\ k_i\ l_i)} \leq 1$ represents films with randomly oriented crystallites, while $TC_{(h_i\ k_i\ l_i)} > 1$ indicate

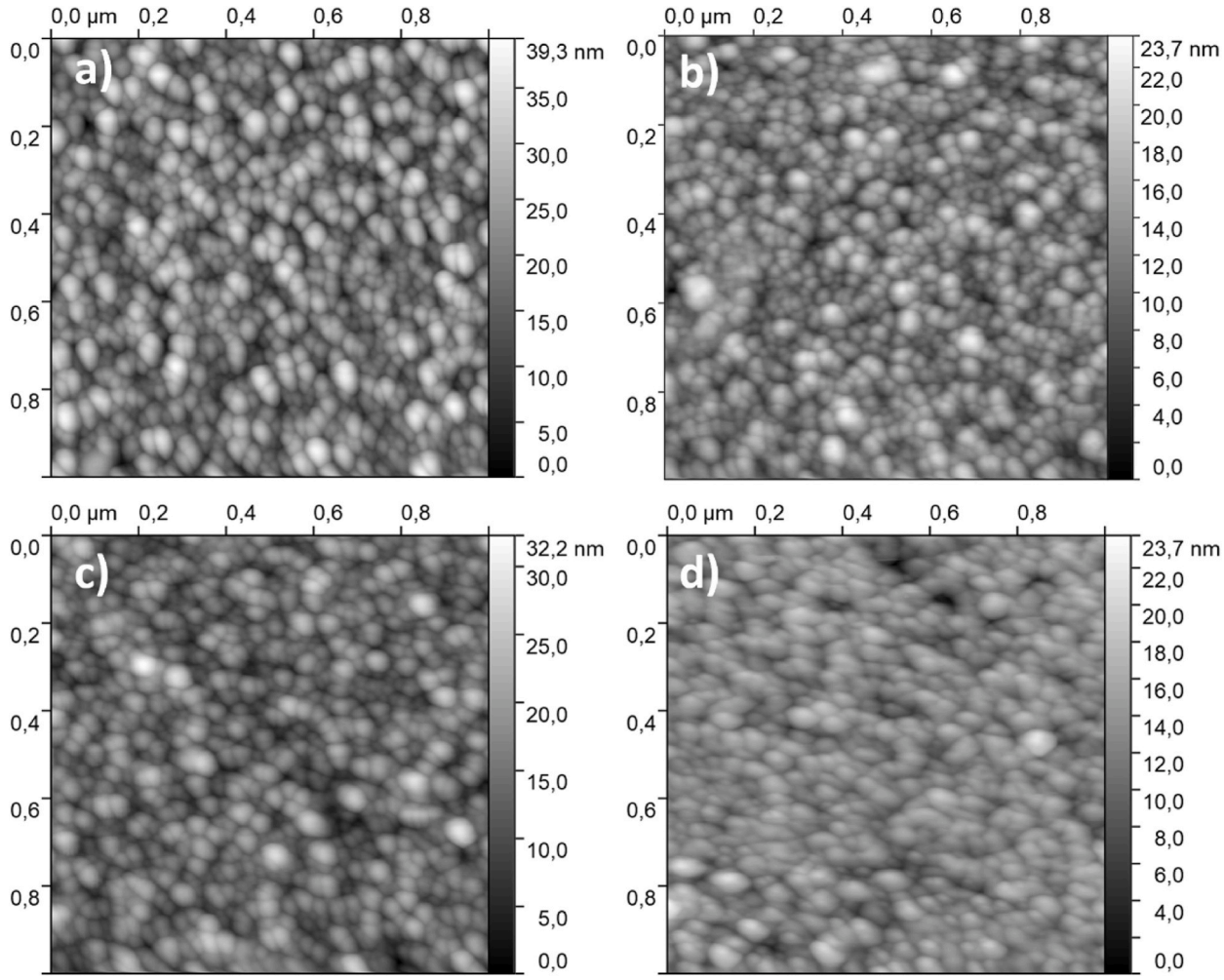

Fig. 7. Atomic force microscopy (AFM) image of tin oxide thin films. Area size is 1 µm × 1 µm with 512 points in each x & y resulting in 2 nm step size. a) SnO_2 film with 270 °C substrate at 25 sccm O_2 flow rate; b) Ta doped SnO_2 film with 270 °C substrate at 25 sccm O_2 flow rate; c) SnO_2 film with 400 °C substrate at 25 sccm O_2 flow rate; d) Ta doped SnO_2 film with 400 °C substrate at 25 sccm O_2 flow rate.

Table 3
Statistics from AFM measurements on a 1 µm × 1 µm large area for samples deposited at 25 sccm oxygen flow.

Sample	Roughness (RMS)	Average Grain Size	Average Aspect Ratio
SnO_2 @ 270 °C	6,02 nm	32,9 nm	2,36
SnO_2 @ 400 °C	4,08 nm	35,4 nm	2,35
SnO_2: Ta @ 270 °C	3,01 nm	31,0 nm	2,37
SnO_2: Ta @ 400 °C	2,32 nm	35,9 nm	2,72

the abundance of grains oriented in this given (hkl) direction. For SnO films deposited by gas flow sputtering (GFS) process, (002) orientation growth rate is the highest orientation and one preferred orientation for epitaxy growth. For SnO_2 films, (200) is the one potential preferred orientation to grow in sputtering process compared with other orientations.

To better understand the effect of substrate temperature and Ta doping on film growth structure, surface morphology and cross section were done with undoped SnO_2 and Ta doped SnO_2 films deposited at 25 sccm oxygen flow rate with different substrate temperature, which is shown in Fig. 6. High substrate temperature revealed larger grain size, and Ta doping has a strong influence on the film growth, which could be observed in cross section. For undoped SnO_2 film deposited with 270 °C substrate, the whole layer grown not homogeneously, part of the film formed like nanoparticles stacked together on glass substrate, which was marked with red dash area 1 and area 2 in Fig. 6a. With the increasing of substrate temperature, film grown as crystal on glass substrate, but the grown process was not uniformly, in the red dash marked area 3 near SnO_2 film surface, nanoparticles could be observed, and the fracture is very rough, not smooth like other films, which is shown in Fig. 6c. With Ta doping, film crystal grows like columns and grown

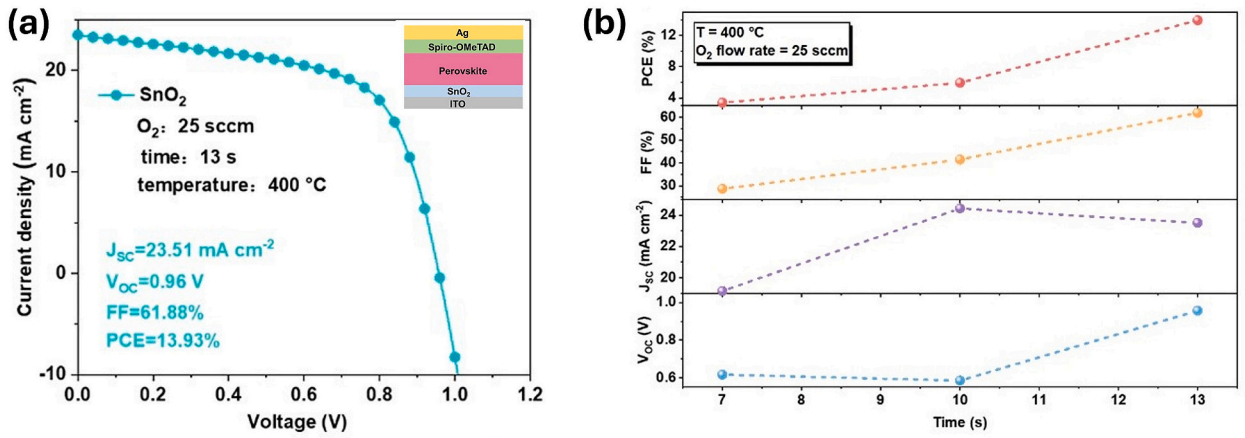

Fig. 8. (a) The J-V curves of the device based on SnO_2 as ETL in perovskite solar cell. Insert is device architecture of planar perovskite solar cell. (b) The change of PCE, FF, $J_{SC,}$ and V_{OC} with O_2 flow rate at 25 sccm and O_2 flow time.

uniformly from the surface of glass substrate, which are shown in Fig. 6b and d. Related with these film XRD pattern and electrical property, it could be inferred that there are two possible ways of Ta contribution in doped SnO_2 films, one is Ta incorporation in SnO_2 cell, and another is on grain boundary to affect grain boundary mobility and growth process. With WDXS measurement it found that atom ratio of Ta decreased from 2.11 % to 1.87 % with the substrate temperature increased from 270 °C to 400 °C.

To investigate lateral grain size and the corresponding roughness AFM measurements are performed in a $1 \times 1\ \mu m^2$ large aera of the SEM samples. For data correction the first order polynom was applied line by line. In general AFM fits the SEM from Fig. 6 and common grain shapes are measured. Overall, the four samples are quite similar in size and shape of the grains. As seen from Fig. 7 there are larger grains (up to 60–80 nm) accompanied by many smaller grains (20–30 nm) in between. These larger grains are almost double in height in respect to surrounding surface. Table 3 lists the root mean square roughness, average grain size and aspect ratio. On the undoped samples roughness is higher by almost factor 2 compared to the Ta doped samples. With increasing temperature, the roughness is reduced and simultaneously the grain size is increased in doped and undoped case, respectively. The shape, indicated by the aspect ratio, stays the same, except for the high temperature Ta doped case. Here a further increase in the aspect ratio is observed.

We fabricated regular n-i-p perovskite solar cells (PSCs) using tin oxides film as electron transport layer (ETL), which is shown in Fig. 8. It is evident that, compared with SnO_2 deposited with 270 °C substrate, the PSCs based on undoped SnO_2 deposited with 400 °C substrate exhibited a higher PCE of 13.93 %, corresponding V_{OC} of 0.96 V, J_{SC} of 23.51 mA cm^{-2}, and FF of 61.88 %. Since SnO_2 film with 400 °C substrate has a low surface roughness, it is ascribed to a reduced concentration of traps at the interface between the SnO_2 interlayer and the active layer [55].

4. Summary

In this work, the sputtering process of reactive gas flow sputtering was introduced to deposit n-type tin oxide films, and the relationship between film structure and optical and electrical properties is discussed in detail. The Ta doping effect was influenced by substrate temperature and O_2 flow rate used in the sputtering process, two key parameters for optimizing and producing tin oxide films by GFS technology. Substrate temperature at 270 °C and O_2 flow rate at 20 and 25 sccm could produce good quality SnO_2: Ta films. Ta doping at 270 °C substrate temperature resulting in a minimum resistivity of $4.01 \times 10^{-3}\ \Omega$ cm, a significant reduction in transmittance in the infrared range, leading to higher carrier concentration in SnO_2: Ta films ($\sim 10^{20}$ cm^{-3}) compared to SnO_2 films ($\sim 10^{19}$ cm^{-3}). From XRD result, Ta doping increased film crystallinity with the increasing of O_2 flow rate up to 25 sccm, followed by degradation beyond 25 sccm due to excess oxygen vacancies. With a higher substrate temperature, the effect of Ta doping on film electrical property is not effective, due to Ta doping works as scattering center and the composition of intermediate tin oxide was observed in tin oxide film, however, Ta doping still increased carrier concentration in SnO_2:Ta films (4.54×10^{20} cm^{-3}) compared to SnO_2 films (2.29×10^{20} cm^{-3}) at 25 sccm O_2 flow rate. A higher substrate temperature could reach a lower refractive index of 1.92. The future pursuits will involve optimizing the Ta doping concentration on film structure and investigating epitaxial growth of SnO_2: Ta films on crystalline substrates, capitalizing on the high plasma density and low energetic ion bombardment facilitated by GFS technology.

Data availability statement

Data will be made available on request.

Declaration of competing interest

The authors declare that they have no known competing financial interests or personal relationships that could have appeared to

influence the work reported in this paper.

Acknowledgments

We sincerely thank the support from Technical University Berlin, the support for the X-ray diffractometer used by the Deutsche Forschungsgemeinschaft (DFG, German Research Foundation) – grant number AOBJ 649257, acknowledge the computational resources of PVcomB, Helmholtz-Zentrum Berlin für Materialien und Energie GmbH (HZB). We also thank the cooperation with the Laboratory for advanced functional materials, the Xiamen Institute of rare earth materials, the Haixi Institute, the Chinese Academy of Sciences for applying tin oxide based on perovskite solar cells, and the financial support from the National Natural Science Foundation of China (21975260).

References

[1] W. Beyer, J. Hüpkes, H. Stiebig, Transparent conducting oxide films for thin film silicon photovoltaics, Thin Solid Films 516 (2007) 147–154, https://doi.org/10.1016/j.tsf.2007.08.110.
[2] S.M. Rozati, S.A.M. Ziabari, A review of various single layer, bilayer, and multilayer TCO materials and their applications, Mater. Chem. Phys. 292 (2022) 126789, https://doi.org/10.1016/j.matchemphys.2022.126789.
[3] K. Chopra, I. Kaur, Thin Film Device Applications, Springer US, 1983, https://doi.org/10.1007/978-1-4613-3682-2.
[4] S. Bohme, B. Philippe, K. Edstrom, L. Nyholm, Photoelectron spectroscopic evidence for overlapping redox reactions for SnO2 electrodes in lithium-ion batteries, J. Phys. Chem. C 121 (2017) 4924–4936, https://doi.org/10.1021/acs.jpcc.7b01529.
[5] M. Shestakova, M. Vinatoru, T.J. Mason, E. Iakovleva, M. Sillanpää, Sonoelectrochemical degradation of formic acid using Ti/Ta2O5-SnO2 electrodes, J. Mol. Liq. 223 (2016) 388–394, https://doi.org/10.1016/j.molliq.2016.08.054.
[6] S. Yu, X. Liu, H. Dong, X. Wang, L. Li, Flexible high-performance SnO2/AgNWs bilayer transparent conductors for flexible transparent heater applications, Ceram. Int. 47 (2021) 20379–20386, https://doi.org/10.1016/j.ceramint.2021.04.046.
[7] Y.-X. Li, Z. Guo, Y. Su, X.-B. Jin, X.-H. Tang, J.-R. Huang, X.-J. Huang, M.-Q. Li, J.-H. Liu, Hierarchical morphology-dependent gas-sensing performances of three-dimensional SnO2 nanostructures, ACS Sens. 2 (2017) 102–110, https://doi.org/10.1021/acssensors.6b00597.
[8] E. Brunet, T. Maier, G.C. Mutinati, S. Steinhauer, A. Köck, C. Gspan, W. Grogger, Comparison of the gas sensing performance of SnO2 thin film and SnO2 nanowire sensors, Sensor. Actuator. B Chem. 165 (2012) 110–118, https://doi.org/10.1016/j.snb.2012.02.025.
[9] L. Qiu, Z. Liu, L.K. Ono, Y. Jiang, D.-Y. Son, Z. Hawash, S. He, Y. Qi, Scalable fabrication of stable high efficiency perovskite solar cells and modules utilizing room temperature sputtered SnO2 electron transport layer, Adv. Funct. Mater. 29 (2019) 1806779, https://doi.org/10.1002/adfm.201806779.
[10] Q. Jiang, X. Zhang, J. You, SnO2: a wonderful electron transport layer for perovskite solar cells, Small 14 (2018) 1801154, https://doi.org/10.1002/smll.201801154.
[11] S. Yu, J. Li, L. Zhao, M. Wu, H. Dong, L. Li, Simultaneously enhanced performances of flexible CuNW networks by covering ATO layer for polymer solar cells, Sol. Energy Mater. Sol. Cell. 221 (2021) 110885, https://doi.org/10.1016/j.solmat.2020.110885.
[12] K. Zhang, Y. Wu, W. Wang, B. Li, Y. Zhang, T. Zuo, Recycling indium from waste LCDs: a review, Resour. Conserv. Recycl. 104 (2015) 276–290, https://doi.org/10.1016/j.resconrec.2015.07.015.
[13] D.A. Keller, H.-N. Barad, E. Rosh-Hodesh, A. Zaban, D. Cahen, Can fluorine-doped tin Oxide, FTO, be more like indium-doped tin oxide, ITO? Reducing FTO surface roughness by introducing additional SnO2 coating, MRS Commun 8 (2018) 1358–1362, https://doi.org/10.1557/mrc.2018.179.
[14] S. Yu, X. Liu, P. Yang, L. Zhao, H. Dong, C. Wu, X. Li, J. Xiong, Highly stable silver nanowire networks with tin oxide shells for freestanding transparent conductive nanomembranes through all-solution processes, Chem. Eng. J. 446 (2022) 137481, https://doi.org/10.1016/j.cej.2022.137481.
[15] J. Ma, X. Zheng, H. Lei, W. Ke, C. Chen, Z. Chen, G. Yang, G. Fang, Highly efficient and stable planar perovskite solar cells with large-Scale manufacture of E-beam evaporated SnO2 toward commercialization, Sol. RRL 1 (2017) 1700118, https://doi.org/10.1002/solr.201700118.
[16] R. Mientus, M. Weise, S. Seeger, R. Heller, K. Ellmer, Electrical and optical properties of amorphous SnO2: Ta films, prepared by dc and rf magnetron sputtering: a systematic study of the influence of the type of the reactive gas, Coatings 10 (2020) 204, https://doi.org/10.3390/coatings10030204.
[17] A. Marzec, M. Radecka, W. Maziarz, A. Kusior, Z. Pedzich, Structural, optical and electrical properties of nanocrystalline TiO2, SnO2 and their composites obtained by the sol–gel method, J. Eur. Ceram. Soc. 36 (2016) 2981–2989, https://doi.org/10.1016/j.jeurceramsoc.2015.12.046.
[18] M. Kwoka, L. Ottaviano, M. Passacantando, S. Santucci, G. Czempik, J. Szuber, XPS study of the surface chemistry of L-CVD SnO2 thin films after oxidation, Thin Solid Films 490 (2005) 36–42, https://doi.org/10.1016/j.tsf.2005.04.014.
[19] J.-H. Kwon, M. Kim, S.-H. Hong, others, Structural characteristics of epitaxial SnO2 films deposited on a-and m-cut sapphire by ALD, J. Cryst. Growth 322 (2011) 33–37, https://doi.org/10.1016/j.jcrysgro.2011.03.004.
[20] L.B. Knight Jr., S.T. Cobranchi, B.W. Gregory, E. Earl, Reinvestigation of the aluminum hydride (AlH+ and AlD+) cation radicals by ESR in argon matrices at 4 K: Generation by reactive laser sputtering, J. Chem. Phys. 86 (1987) 3143–3150, https://doi.org/10.1063/1.452025.
[21] S. Yu, W. Zhang, L. Li, D. Xu, H. Dong, Y. Jin, Transparent conductive Sb-doped SnO2/Ag multilayer films fabricated by magnetron sputtering for flexible electronics, Acta Mater. 61 (2013) 5429–5436, https://doi.org/10.1016/j.actamat.2013.05.031.
[22] S.C. Dixon, D.O. Scanlon, C.J. Carmalt, I.P. Parkin, n-Type doped transparent conducting binary oxides: an overview, J Mater Chem C Mater 4 (2016) 6946–6961, https://doi.org/10.1039/C6TC01881E.
[23] B.A.D. Williamson, T.J. Featherstone, S.S. Sathasivam, J.E.N. Swallow, H. Shiel, L.A.H. Jones, M.J. Smiles, A. Regoutz, T.-L. Lee, X. Xia, others, Resonant Ta doping for enhanced mobility in transparent conducting SnO2, Chem. Mater. 32 (2020) 1964–1973, https://doi.org/10.1021/acs.chemmater.9b04845.
[24] B. Bissig, T. Jäger, L. Ding, A.N. Tiwari, Y.E. Romanyuk, Limits of carrier mobility in Sb-doped SnO2 conducting films deposited by reactive sputtering, Apl. Mater. 3 (2015) 62802, https://doi.org/10.1063/1.4916586.
[25] S. Yu, L. Li, W. Zhang, H. Dong, D. Xu, Y. Jin, Investigation of low resistance transparent F-doped SnO2/Cu bi-layer films for flexible electronics, Vacuum 102 (2014) 43–47, https://doi.org/10.1016/j.vacuum.2013.10.021.
[26] S. Yu, W. Zhang, L. Li, D. Xu, H. Dong, Y. Jin, Optimization of SnO2/Ag/SnO2 tri-layer films as transparent composite electrode with high figure of merit, Thin Solid Films 552 (2014) 150–154, https://doi.org/10.1016/j.tsf.2013.11.109.
[27] S. Yu, P. Yang, B. Wang, N. Zhang, C. Wu, High-temperature resistance of flexible transparent conductive films based on Ag@SnO2 core-shell nanowires for 300 °C, Mater. Lett. 328 (2022) 133031, https://doi.org/10.1016/j.matlet.2022.133031.
[28] M. Wu, H. Zheng, X. Li, S. Yu, Highly transparent low resistance ATO/AgNWs/ATO flexible transparent conductive thin films, Ceram. Int. 46 (2020) 4344–4350, https://doi.org/10.1016/j.ceramint.2019.10.157.
[29] H. Dong, S. Yu, L. Song, X. Wang, C. Wu, Fabrication of high-quality flexible transparent conductive thin films with a Nb2O5/AgNWs/Nb2O5 sandwich structure, Ceram. Int. 48 (2022) 15348–15354, https://doi.org/10.1016/j.ceramint.2022.02.068.
[30] Y. Zhou, L. Zhao, N. Zhang, C. Chang, Z. Song, W. An, Q. Dong, S. Yu, Self-assembled growing ultrathin Ag@NiO core-shell nanowires for stable freestanding transparent conductive colorless polyimide nanomembranes, J. Alloys Compd. 935 (2023) 168012, https://doi.org/10.1016/j.jallcom.2022.168012.
[31] S. Yu, X. Liu, M. Wu, H. Dong, X. Wang, L. Li, All-solution-processed molybdenum oxide-encapsulated silver nanowire flexible transparent conductors with improved conductivity and adhesion, ACS Appl. Mater. Interfaces 13 (2021) 14470–14478, https://doi.org/10.1021/acsami.0c22324.
[32] S. Yu, L. Zhao, R. Liu, C. Zhang, H. Zheng, Y. Sun, L. Li, Performance enhancement of Cu-based AZO multilayer thin films via graphene fence engineering for organic solar cells, Sol. Energy Mater. Sol. Cell. 183 (2018) 66–72, https://doi.org/10.1016/j.solmat.2018.04.008.

[33] S. Yu, Y. Liu, H. Zheng, L. Li, Y. Sun, Improved performance of transparent-conducting AZO/Cu/AZO multilayer thin films by inserting a metal Ti layer for flexible electronics, Opt Lett 42 (2017) 3020, https://doi.org/10.1364/OL.42.003020.
[34] S. Yu, L. Li, X. Lyu, W. Zhang, Preparation and investigation of nano-thick FTO/Ag/FTO multilayer transparent electrodes with high figure of merit, Sci. Rep. 6 (2016) 20399, https://doi.org/10.1038/srep20399.
[35] S. Yu, L. Song, C. Wu, L. Li, Enhanced conductivity and stability of Cu-embedded zinc tin oxide flexible transparent conductive thin films, Ceram. Int. 48 (2022) 15925–15931, https://doi.org/10.1016/j.ceramint.2022.02.133.
[36] S. Yu, L. Li, D. Xu, H. Dong, Y. Jin, Characterization of SnO2/Cu/SnO2 multilayers for high performance transparent conducting electrodes, Thin Solid Films 562 (2014) 501–505, https://doi.org/10.1016/j.tsf.2014.04.064.
[37] B. Szyszka, W. Dewald, S.K. Gurram, A. Pflug, C. Schulz, M. Siemers, V. Sittinger, S. Ulrich, Recent developments in the field of transparent conductive oxide films for spectral selective coatings, electronics and photovoltaics, Curr. Appl. Phys. 12 (2012) S2–S11, https://doi.org/10.1016/j.cap.2012.07.022.
[38] B. Szyszka, Magnetron sputtering of ZnO films, in: Transparent Conductive Zinc Oxide, Springer, 2008, pp. 187–233, https://doi.org/10.1007/978-3-540-73612-7.
[39] T. Kälber, Hohlkathoden-Gasflußputttern zur Verschleißschutzbeschichtung von Kunststoffen, TU, Braunschweig, 1998.
[40] B. Szyszka, Reaktives Magnetronsputtern von transparenten und leitfähigen Oxidschichten, JLU Giessen, 1999.
[41] N. Alktash, R. Muydinov, D. Erfurt, M. Hartig, W. Gajewski, B. Szyszka, Indigenous facility of the unipolar pulsed power generation for gas flow sputtering of titania films, Rev. Sci. Instrum. 94 (2023), https://doi.org/10.1063/5.0148807.
[42] B. Stjerna, E. Olsson, C.G. Granqvist, Optical and electrical properties of radio frequency sputtered tin oxide films doped with oxygen vacancies, F, Sb, or Mo, J. Appl. Phys. 76 (1994) 3797–3817, https://doi.org/10.1063/1.357383.
[43] M.A. Ponce, C.M. Aldao, M.S. Castro, Influence of particle size on the conductance of SnO2 thick films, J. Eur. Ceram. Soc. 23 (2003) 2105–2111, https://doi.org/10.1016/S0955-2219(03)00037-2.
[44] M. Weidner, J. Jia, Y. Shigesato, A. Klein, Comparative study of sputter-deposited SnO2 films doped with antimony or tantalum, Phys. Status Solidi 253 (2016) 923–928, https://doi.org/10.1002/pssb.201552720.
[45] H.T. Tung, T.P. Nguyen, P.D. Huu, T. Le, Optical, electrical, and structural properties of Ta-doped SnO2 films against substrate temperature using direct current magnetron sputtering, Surface. Interfac. 23 (2021) 100943, https://doi.org/10.1016/j.surfin.2021.100943.
[46] M. Weidner, J. Brötz, A. Klein, Sputter-deposited polycrystalline tantalum-doped SnO2 layers, Thin Solid Films 555 (2014) 173–178, https://doi.org/10.1016/j.tsf.2013.05.147.
[47] T.J. Featherstone, J.E.N. Swallow, J.D. Major, K. Durose, T.D. Veal, Transparent Ta doped SnO 2 films deposited by RF co-sputtering, in: 2018 IEEE 7th World Conference on Photovoltaic Energy Conversion (WCPEC), A Joint Conference of 45th IEEE PVSC, 28th PVSEC & 34th EU PVSEC), 2018, pp. 2980–2984, https://doi.org/10.1109/PVSC.2018.8547755.
[48] N.M. Nguyen, M.Q. Luu, M.H. Nguyen, D.T. Nguyen, V.D. Bui, T.T. Truong, V.T. Pham, T. Nguyen-Tran, Synthesis of tantalum-doped tin oxide thin films by magnetron sputtering for photovoltaic applications, J. Electron. Mater. 46 (2017) 3667–3673, https://doi.org/10.1007/s11664-017-5296-0.
[49] M.F. Al-Kuhaili, Co-sputtered tantalum-doped tin oxide thin films for transparent conducting applications, Mater. Chem. Phys. 257 (2021) 123749, https://doi.org/10.1016/j.matchemphys.2020.123749.
[50] C.R. Onyeagba, M. Islam, P.K.D.V. Yarlagadda, T. Tesfamichael, Investigating the properties of tin-oxide thin film developed by sputtering process for perovskite solar cells, Mater Renew Sustain Energy 12 (2023) 31–37, https://doi.org/10.1007/s40243-022-00226-z.
[51] Y. Zakaria, B. Aïssa, T. Fix, S. Ahzi, S. Mansour, A. Slaoui, Moderate temperature deposition of RF magnetron sputtered SnO2-based electron transporting layer for triple cation perovskite solar cells, Sci. Rep. 13 (2023) 9100, https://doi.org/10.1038/s41598-023-35651-1.
[52] R.W.G. Wyckoff, Interscience publishers, new york, new york rocksalt structure, Crystal Structures 1 (1963) 85–237.
[53] W.H. Baur, Über die verfeinerung der kristallstrukturbestimmung einiger vertreter des rutiltyps: TiO2, SnO2, GeO2 und MgF2, Acta Crystallogr. 9 (1956) 515–520, https://doi.org/10.1107/S0365110X56001388.
[54] C. Guillén, J. Herrero, P-type SnO thin films prepared by reactive sputtering at high deposition rates, J. Mater. Sci. Technol. 35 (2019) 1706–1711, https://doi.org/10.1016/j.jmst.2019.03.034.
[55] Z. Ma, Z. Tang, E. Wang, M.R. Andersson, O. Inganäs, F. Zhang, Influences of surface roughness of ZnO electron transport layer on the photovoltaic performance of organic inverted solar cells, J. Phys. Chem. C 116 (2012) 24462–24468, https://doi.org/10.1021/jp308480u.